

Topological two-parameter charge pump in a one-dimensional semiconductor nanowire superlatticeJ. Wang,^{1,2} J. F. Liu,³ and C. S. Ting¹¹*Texas Center for Superconductivity and Department of Physics, University of Houston, Houston, Texas 77204, USA*²*School of Physics, Southeast University, Nanjing, 210096, China*³*Department of Physics, School of Physics and Electronic Engineering, Guangzhou University, Guangzhou 510006, China*

(Received 18 February 2019; published 1 August 2019)

We study a possible topological charge pump in a traditional two-parameter pump device, which is based on a one-dimensional (1D) semiconductor nanowire with Rashba spin-orbit interaction. The 1D nanowire has a superlattice structure through periodic folding and the pumping parameters are the two time-dependent Zeeman fields with a phase lag φ between them. It is shown that the Zeeman field can open an energy gap of the nanowire superlattice and the system enters into a topological state. There are two electron charges pumped out adiabatically in a pumping cycle if the Fermi energy resides in the energy gap and φ is not close to $n\pi$ (n , an integer). This originates from the topologically protected interface state forming between the two pumping sources, which evolves with time, resulting in electron charges from one end transported to the other end of the wire. The quantized current direction can be modulated by some system parameters such as the Fermi energy, pumping phase, and the local potential of the device via gate voltage.

DOI: [10.1103/PhysRevB.100.075402](https://doi.org/10.1103/PhysRevB.100.075402)**I. INTRODUCTION**

Adiabatic charge pump is a quantum transport phenomenon in mesoscopic electron systems and has been attracting considerable theoretical and experimental interest for decades [1–9]. When some parameters of the system are changed periodically with time, a finite charge may be transmitted through the system at the end of the pumping cycle without any external bias. Much effort has been devoted to the quantized pump in which an integer number of charges are pumped out in a cycle, because the pumping quantization is quite desirable in building a standard of electric current [4–6]. The Coulomb blockade effect as a usual routine to acquire the pumping quantization was extensively studied [10–14] in quantum-dot systems and this has been successfully demonstrated in both theoretical and experimental research. In the noninteracting electron system, the quantized charge pump mostly refers to the Thouless topological pump [15], in which a one-dimensional (1D) moving potential can pump out integral charges in a cycle when the Fermi energy lies in the energy gap opened by the moving potential. This 1D periodic system is topological and the pumped charge number in each cycle equals the topological invariant of the system [16–20]. Recently, several research groups [21–24] have independently observed such quantized pump in 1D optical superlattice or cold-atom systems. However, it is still a challenge in solid electron systems since one needs to precisely control the moving potential felt by electrons.

For a general two-parameter pump device where the two time-dependent potentials have a phase lag φ between them, it is hard to obtain the pumping quantization in the noninteracting electron systems even from a theoretical aspect. Brouwer [3] pointed out that the pumped current in the adiabatic limit is proportional to the geometric area circled by time-dependent parameters and, in the bilinear approximation,

the current has the formation, $I \sim \sin \varphi$, which seems far from quantization. Some harsh requirements were concluded in literature [25–28] to realize a quantized pump, which is based on the resonant tunneling effect of electrons, i.e., electrons can perfectly tunnel through the pumping device in a narrow parameter region with the transmission $\mathcal{T} = 1$ but surrounded by zero transmissions, $\mathcal{T} = 0$.

In a previous work [29], two authors presented a pumping protocol to realize the pumping quantization in a two-parameter pump device that is based on the Dirac electrons of graphene: If the pumping potentials (the staggered lattice potential in graphene) could make the original system enter into a topological phase, a topological interface state forming between the two pumping sources would lead to the pumping quantization. Whether such a pumping protocol is valid in the non-Dirac electron systems or in the traditional semiconductor systems is an open question and this motivates us to further study the possible quantized two-parameter charge pumping based on non-Dirac electrons of semiconductor materials.

Given the fact that a perpendicular Zeeman field can break the crossing of the two spin bands of a Rashba spin-orbit interaction media [30,31], we consider in this paper a 1D nanowire superlattice (NWS) as the pumping device model and the two time-dependent Zeeman fields as the pumping potentials. The Zeeman field can directly make the NWS open an energy gap and the system enters into a topological insulating phase from a metallic phase. We will show that the quantized pump is possible with integral charges pumped out in a cycle as long as the Fermi energy is located in the opened energy gap. The integer-charge moving is due to the time evolution of the emergent interface state forming in real space between the two pumping sources. The quantization can also be modulated by some system parameters such as the pumping phase and the local potential via gate voltage.

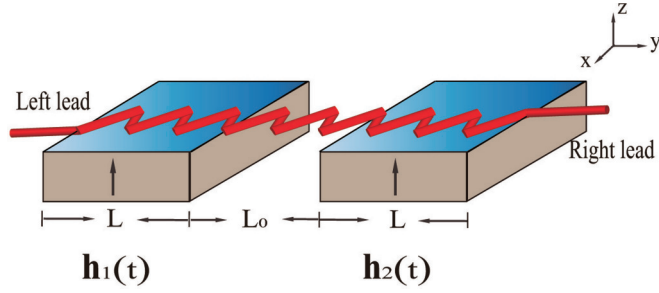


FIG. 1. Schematic of a two-parameter pump device. A folding one-dimensional semiconductor nanowire superlattice is immersed within the two separated time-dependent Zeeman exchange fields, which can be from either magnetic proximity effect or a direct magnetic field, $\mathbf{h}_1(t) = [0, 0, h_z \cos(\omega t)]$ and $\mathbf{h}_2(t) = [0, 0, h_z \cos(\omega t + \varphi)]$. h_z represents the z -directed Zeeman field magnitude while the whole device lies in the xy plane. The pump device is connected with electrodes through the left (L) and right (R) leads. The two Zeeman region lengths are assumed L and the distance between them is L_0 .

The remainder of the paper is laid out as follows. In Sec. II, we present the pump device model and analyze the possible topological phase of the NWS under a Zeeman field. In Sec. III, we will focus on the calculation of the pumped current and discuss the physics origin of the pumping quantization. In the final section, we will discuss possible measurement of the proposed two-parameter quantized pump and draw a brief conclusion.

II. TOPOLOGY OF NANOWIRE SUPERLATTICE

We consider a 1D semiconductor nanowire with a strong Rashba spin-orbit interaction as the base material of the pump device. The nanowire is assumed to be periodically folded or bent to form a NWS structure as shown schematically in Fig. 1. The two time-dependent Zeeman fields, $\mathbf{h}_1(t)$ and $\mathbf{h}_2(t)$, are taken as the pumping parameters separated in real space by a normal region L_0 (without any applied Zeeman field). The whole pumping setup connects with the outside world via the left and right leads, and there is no bias applied onto the device. The possible current can merely come from the perturbation of time-dependent Zeeman fields. The system Hamiltonian in a lattice representation reads

$$H = H_0 + V(t), \quad (1)$$

$$H_0 = -\gamma \sum_{n\sigma} C_{n+1,\sigma}^\dagger C_{n,\sigma} + it_{\text{so}} \sum_{n\alpha\beta} C_{n+1,\alpha}^\dagger (\sigma_n)_{\alpha\beta} C_{n,\beta} + \text{H.c.}, \quad (2)$$

$$V(t) = \sum_{n\alpha\beta} C_{n,\alpha}^\dagger [\mathbf{h}_1(t)\Theta_1(n) + \mathbf{h}_2(t)\Theta_2(n)] \cdot \boldsymbol{\sigma} C_{n,\beta}. \quad (3)$$

Here, H_0 describes the time-independent NWS system and $V(t)$ is the pumping-source term. The first term of H_0 is the electron hopping between the nearest-neighboring sites, γ is the hopping energy, $C_{n\sigma}^\dagger$ ($C_{n\sigma}$) is the creation (annihilation) operator of electrons at the n th site with spin σ (α, β).

The second term of H_0 stands for the Rashba spin-orbit interaction with its strength t_{so} , $\sigma_n = \sigma_x \sin \theta_n + \sigma_y \cos \theta_n$ is the local Rashba field direction with θ_n being the bond direction. As is known, the Rashba field direction is perpendicular to the momentum direction of electrons, and it shall be site (n) independent in the 1D straight NW case. The $V(t)$ term of Eq. (3) represents the time-dependent Zeeman fields, which are simply assumed along the z direction perpendicular to the NWS plane because this magnetization direction can lead to a sizable energy gap of the NWS electron band, $\Theta_1(n) = \Theta(n)\Theta(L-n)$ and $\Theta_2(n) = \Theta(n-L-L_0)\Theta(2L+L_0-n)$ with Θ being the Heaviside step function, so the two Zeeman fields are limited to the separated space as shown in Fig. 1. $\mathbf{h}_1(t) = [0, 0, h_z \cos(\omega t)]$ and $\mathbf{h}_2(t) = [0, 0, h_z \cos(\omega t + \varphi)]$, ω is the pumping frequency and, in the adiabatic limit, it is assumed to be infinitely small ($\omega \rightarrow 0$); t is the time argument, φ is the pumping phase difference, and h_z is the strength of the Zeeman field. For simplicity, the two pumping strengths and pumping source sizes are set the same, h_z and L , respectively.

The periodic folding of nanowire here is assumed to merely cause variation of the local Rashba field direction θ_n as well as the reduction of the original Brillouin zone of a straight wire. It was argued in literature [32,33] that the folding can also cause the so-called quantum geometric potential, which in turn can make the folded nanowire enter into a topological phase and even generate a quantized charge pump with the help of a rotating magnetic field [34]. Oppositely, we neglect the quantum geometric potential in this paper so the folded NWS itself without any applied h_z is still in a metallic phase. Because it is believed that such a quantum geometric potential tends to disappear in a realistic sizable device.

We first present a typical NWS to illustrate the electronic structure as well as the possible topological phase within a uniform static Zeeman field h_z . In Fig. 2(a), we choose a NWS of the rectangular wave shape with its periodicity $N_T = 4$, in which the local bond direction is set as $\theta_n = (\pi/2, 0, -\pi/2, 0)$. The electronic structure of such an infinitely long wire is shown in Fig. 2(b). There is no energy gap forming in the case of $h_z = 0$ and the band simply comes from the $1/N_T$ Brillouin-zone folding of a straight nanowire. However, the nontrivial structure is the emergent band crossings at $\pm K$ as marked in dashed red circles, where only the lowest crossings are noted. The crossings are due to the Rashba spin-orbit interaction and are similar to the original band crossing at the band center $ka = 0$. Around the crossing points, $\pm K$, electrons have a linear energy dispersion and can be approximately described as

$$\mathcal{H}_{K(K')} = \pm \hbar v_f \sigma_\theta k + h_z \sigma_z, \quad (4)$$

where σ_θ is the eigenspin of electrons around $\pm K$ but it always lies in the xy plane, v_f is the velocity of electrons, k is the 1D momentum expanded around $\pm K$, and \pm indicates the different chirality of electrons around $+K$ and $-K$, respectively. Here, the \pm chirality represents the opposite spin-momentum dependence around $\pm K$. The $+K$ and $-K$ degeneracy may also be referred to as the twofold valley degeneracy. The first term of the formula above is the same as the low-energy Dirac equation of graphene [35] but the difference is also clear: σ_θ is a real spin lying in the xy plane whereas, in graphene, σ

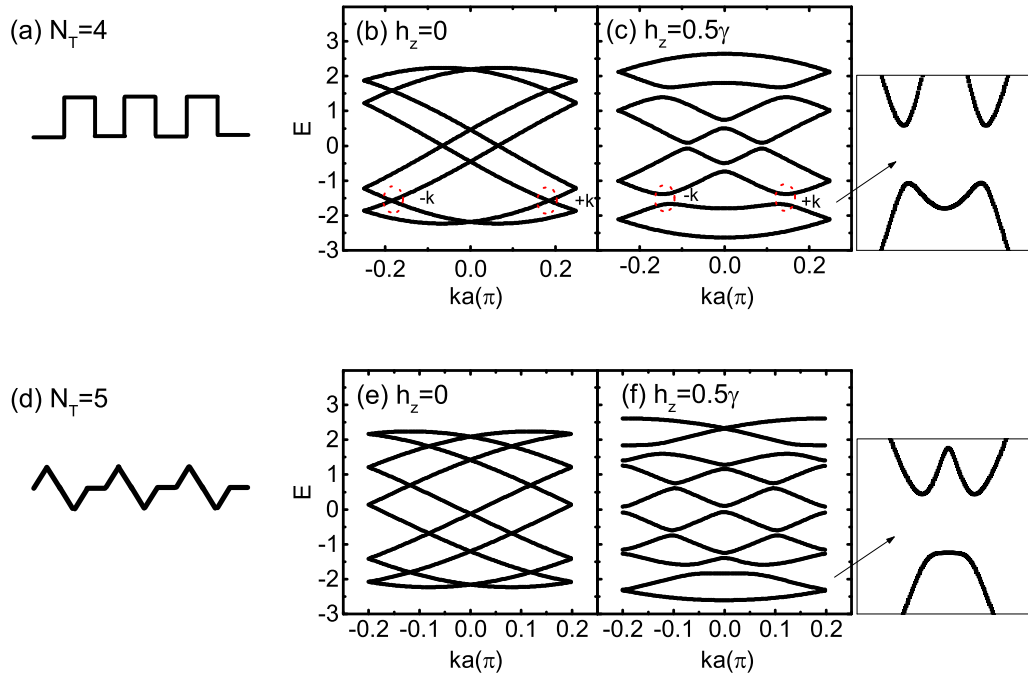


FIG. 2. Electronic band structures of the infinite-long 1D NWS with two different periodicities $N_T = 4$ (a)–(c) and $N_T = 5$ (d)–(f). (a) A rectangle NWS is considered with the bond direction set as $\theta_n = (\pi/2, 0, -\pi/2, 0)$. The energy dispersion $E-ka$ is plotted without (b) or with (c) a single static Zeeman field applied onto the system, where a is the lattice constant. The circle points $\pm K$ stand for the valley degeneracy due to the folding of the 1D NW. (d) The $N_T = 5$ NWS setup is plotted with the bond direction as $(\theta_n = \pi/3, -\pi/3, -\pi/3, \pi/3, 0)$ and the band structures are plotted in (e) and (f). The rightmost insets near (c) and (f) are the lowest energy gaps opened by h_z . The spin-orbit coupling strength is set as $t_{so} = 0.5\gamma$ and $\gamma = 1$ in calculations.

denotes the lattice pseudospin. If a perpendicular exchange field is present like the second term of the above equation, $h_z\sigma_z$, the energy band is expected to exhibit an energy gap and the system enters into a topological phase. This is confirmed by the electronic band in Fig. 2(c) within a nonzero h_z and the original crossing points besides the marked $\pm K$ are all opened now. The lowest energy gap is enlarged for clear viewing in the right inset of Fig. 2(c).

In fact, other NWSs of different folding shapes can lead to the same effect like the band crossing as well as the energy gap opened by the h_z field. In Figs. 2(d)–2(f), a similar situation is shown for the shape of NWSs with $N_T = 5$ [see Fig. 2(d)] and the local lattice bond direction is set as $\theta_n = (\pi/3, -\pi/3, -\pi/3, \pi/3, 0)$. As long as the folding of NWS exists, the *local* spin rotates in real space due to the Rashba spin-orbit interaction. When we choose the local spin direction as the quantum spin axis instead of the h_z direction, the 1D electrons could feel a spatially modulated spiral magnetization, which necessarily gives rise to a topological phase of the system.

As stated above, the linear energy dispersion around $\pm K$ as well as the energy gap opened by h_z in Fig. 2 are superficially the same as the Dirac electrons in a staggered graphene [29]. However, the spin operator here is a real electron spin (measurable quantity) and, thus, the topological state can exhibit the bulk-edge (end) correspondence in a finite-size system. Oppositely, there is no edge state for the staggered graphene where the carbon A and B sites have the opposite static

potentials, even though the system is actually in a quantum valley hall insulator state [36,37].

In Fig. 3(a), we calculate the energy levels of a finite-length NWS as a function of the eigenstate index i and here the wire parameter is the same as that in Fig. 2(c) except for the finite size. There are two isolated energy levels appearing in the original bulk gap of the NWS as clearly shown in the inset of Fig. 3(a). The corresponding wave-function distributions are also plotted in Fig. 3(b) and their localization at the two ends of wire is clearly seen. This indicates that the system is in a topological phase. The fraction-charge state [16,17], which occurs in periodically modulated 1D NW, does not appear here, because both the time reversal symmetry and the central inversion symmetry of the system are broken by the Zeeman field and Rashba spin-orbit interaction, respectively.

Similar to the staggered potential term in graphene systems [37], the h_z term in Eq. (4) here will determine the sign of the topological invariant as well, $\text{sgn}(h_z)$. Therefore, the $+h_z$ and $-h_z$ terms will lead to the different topological phases with the opposite topological invariants. A topological interface state may appear in a nonuniform NWS within an existing domain wall (actually, which is a point in the 1D case) when the system consists of the neighboring $+h_z$ and $-h_z$ regions.

In Fig. 4(a), we carry out the same computation of the energy band of a finite NWS within a half static $-h_z$ and a half static $+h_z$ applied on the NWS. It can be seen that in the original bulk gap, four isolated energy levels appear

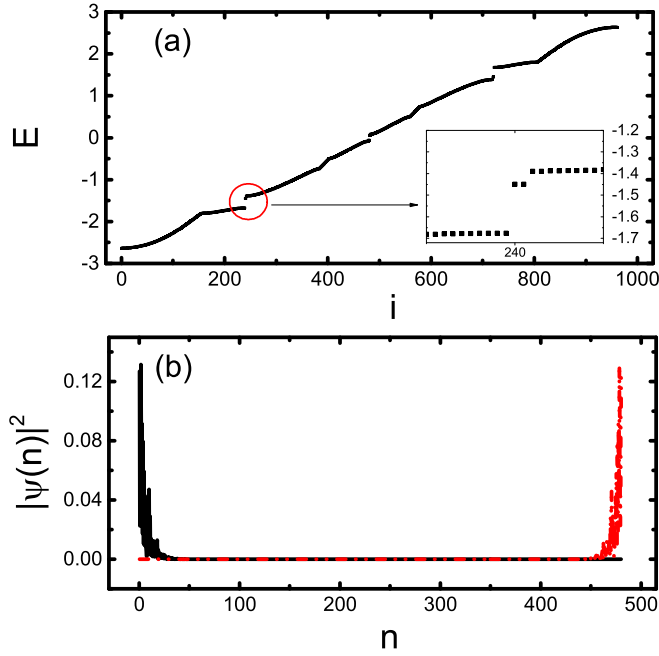


FIG. 3. (a) Eigenvalues $E-i$ of a finite NWS within a nonzero h_z field. The circled energy gap is enlarged in the inset and two isolated energy levels appear. (b) Spatial distribution of the wave functions $|\Psi(n)|^2-n$ of two isolated levels. The two wave functions are separated and localized conspicuously in either end of the NWS. $h_z = t_{so} = 0.5\gamma$, $L(N_T) = 120$, and $N_T = 4$.

[see the enlarged inset of Fig. 4(a)] and two emergent ones should denote the possible interfacial states localizing around the domain wall (point). To confirm this, we plotted the corresponding wave-function distributions of the four isolated energy levels in Fig. 4(b). It is clearly shown that there are two wave functions localizing in the middle of the NWS where the domain wall stands and the other two wave functions are the end states—same as those in Fig. 3(b). Such interface states in the energy gap should be protected by the topology of the system and are expected to exert an effect on the pumping event.

III. PUMPED CURRENT

In this section, we shall calculate the possible pumped current flowing through the device in Fig. 1, which reads in the adiabatic limit [29] as

$$I_s = \frac{e}{2\pi T} \oint dt \text{Tr}[\Gamma G^r \dot{V} G^a]_{ss}, \quad (5)$$

where e is the electron charge, T is the period of the pumping cycle, $s = L, R$ stands for the left or right lead through which the current is flowing toward the electrodes, $G^r = [EI - \tilde{H}(t) - \Sigma_L^r - \Sigma_R^r]^{-1}$ is the retarded Green's function while $G^a = (G^r)^\dagger$ is the advanced one, I is the unit matrix, $\tilde{H}(t)$ is the pumping device Hamiltonian not including the leads, $\dot{V} = dV(t)/dt$, $\Sigma_{L,R}^r$ is the self-energy of the left (right) leads, $\Gamma = i[\Sigma^r - (\Sigma^r)^\dagger]$, and they are time independent. The self-energy here is computed by using a usual recursion method

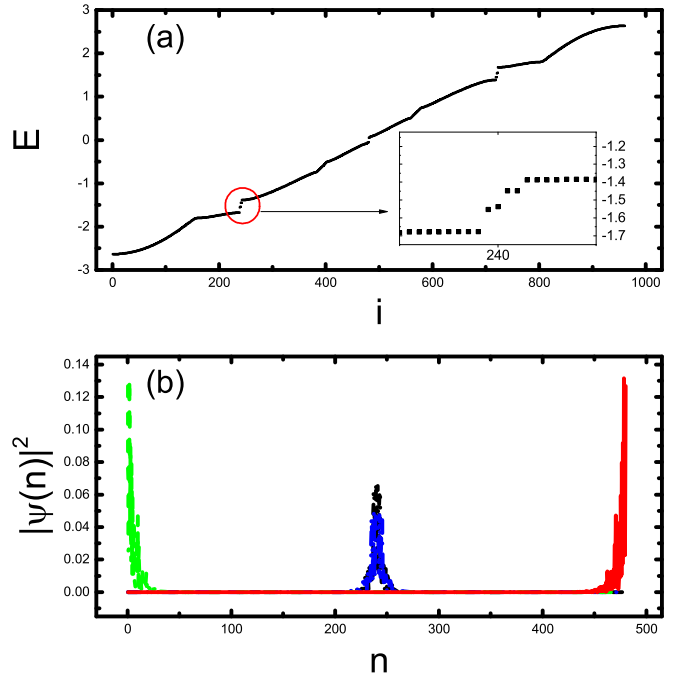


FIG. 4. (a) Eigenvalues $E-i$ of the finite NWS within a half $+h_z$ and the other half $-h_z$ field applied. The circled bulk energy gap is enlarged in the inset and four isolated energy levels appear. (b) Spatial distribution of the wave functions $|\Psi(n)|^2-n$ of four isolated-levels in the energy gap. The two wave functions are localized in either end of the NWS while the other two wave functions are localized at the center of the NWS where the domain interface resides exactly between $+h_z$ and $-h_z$. $h_z = t_{so} = 0.5\gamma$, $L(N_T) = 120$, and $N_T = 4$.

in the lattice model [38]. It is noted that the left and right electrodes can be assumed to be the NWS itself or a normal wire without spin-orbit interaction and periodic folding; the results will stay the same, especially for the quantized pumped current as we will present below.

In the model calculations, we take the hopping energy $\gamma = 1$ as the energy unit and a zero ambient temperature is considered. The NWS with the periodicity $N_T = 4$ is shown to illustrate the pumping current as an example since the other folding-shape NWSs will exhibit the same qualitative results. In Fig. 5(a), the pumped current I_L is presented as a function of the Fermi energy E . Here, the E -axis span represents the bulk energy gap Δ_0 of the NWS and its size is approximately from -1.69γ to -1.39γ estimated around $\pm K$ in Fig. 2(c).

One can see that I_L exhibits a clear quantization platform inside the bulk energy gap, $I = \pm 2e/T$, i.e., an integer number of electron charges ($2e$) are pumped out adiabatically in a pumping cycle. 2 stems from the spin degeneracy but, directly, it is related to the two cross points or *valley* degeneracy ($\pm K$) as shown in the electronic bands (Fig. 2). Outside the platforms, the pumped current is nonquantized and its value may exceed the quantized one $\pm 2e/T$. Although each pumping source (a single lattice point associated with a pumping potential) contributes to the current necessarily smaller than $2e/T$, the total contribution of multiple pumping sources may

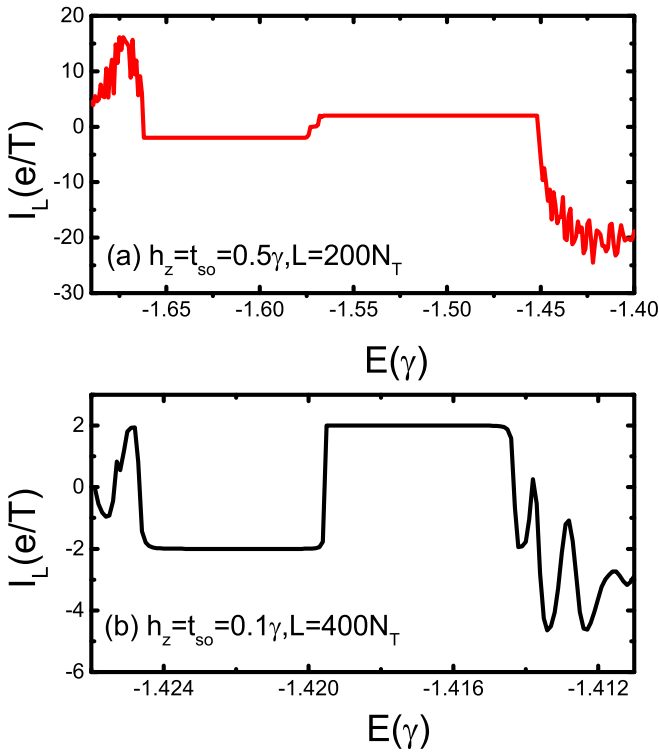


FIG. 5. Pumped current (I_L) as a function of energy E within different spin-orbit and Zeeman field strengths. Here, the energy axis (E) is exactly limited in the bulk energy gap of the NWS opened by a single uniform h_z . Other parameters are $L_0 = 0$ and $\varphi = \pi/2$.

exceed $2e/T$, especially when there is not any collective behavior from the pumping sources like the insulating phase from the pumping potential, the h_z field.

The energy region for the pumping quantization in Fig. 5(a) is a little smaller than the bulk gap, which is defined for the NWS within a single uniform and static h_z field. Obviously, this uniform h_z is not the case for our studied pump device, where two time-dependent Zeeman fields are involved. The quantization of I_L necessitates that E should keep inside the so-called effective energy gap or transport gap in the whole pumping cycle. In other words, the system is insulating and no electron can directly transport through the device instantly. Obviously, the pumping potential phase φ between $\mathbf{h}_1(t)$ and $\mathbf{h}_2(t)$ should play an important role in determining the effective gap energy δ , since neither of them can individually keep gap opening consistently in a cycle T . From the linear Dirac equation [Eq. (4)], one can find an approximate formula, $\delta = \Delta_0 \sqrt{(1 - |\cos \varphi|)/2}$, by assuming Δ_0 to be the original bulk energy gap opened by a single field h_z .

As long as E lies in this effective gap, the pumping current would be quantized no matter how small δ is. This can be seen from Fig. 5(b) where the quantization is still clear for the case of a weak t_{so} and h_z , $t_{so} = h_z = 0.1\gamma$. From another perspective, the energy interval for the pumping quantization is crucially related to the magnitudes of t_{so} and h_z . Beside them, the bulk energy gap is also influenced by the $\partial\theta_n/\partial n$ magnitude, especially when $N_T a$ is in the atomic size. However, $\partial\theta_n/\partial n$ approaches zero as $N_T a$ is above the order of

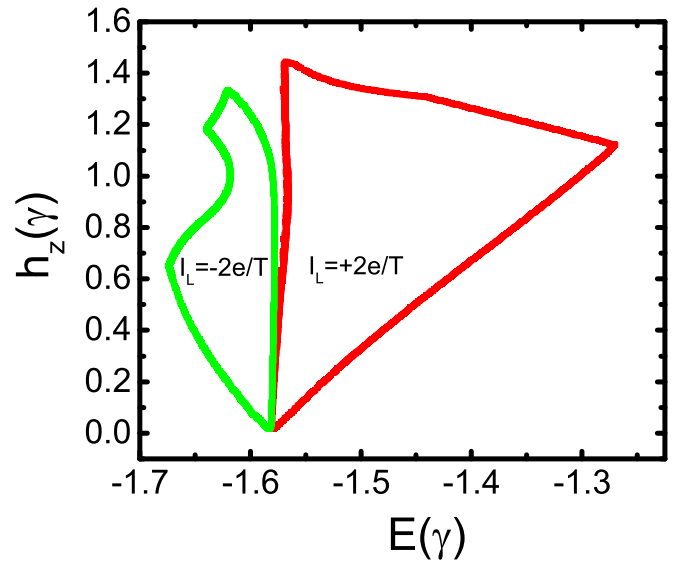


FIG. 6. Quantized pump results of I_L in the parameter ($E-h_z$) space. Outside of two self-closed circles, the pumped current I_L is nonquantized. Parameters are the same as those in Fig. 5(a).

magnitude of 10 nm so it will not heavily affect the bulk energy gap of the NWS. In the calculation of Fig. 5(b), a smaller bulk energy gap will cause difficulty in numerical convergence of the integration [Eq. (5)], so a larger pumping region is assumed as $L = 400N_T$ in our calculations of Fig. 5(b). This is due to the quantum tunneling effect of electrons through the small energy gap, resulting in nonzero transmission. The opposite case of a larger h_z may be invalid for generating the pumping quantization.

In fact, there is no quantized I_L when h_z is large enough. From the band structure in Fig. 2(c), one can see that the two crossing points ($\pm K$) should merge together at the band center $ka = 0$ in a very large h_z and even the system may be in the half-metal state. Subsequently, the valley degree of freedom due to the superlattice structure will disappear and no possible interface state can form to generate the possible quantized I_L . The corresponding quantized-pump region in the parameter space is plotted in Fig. 6, where inside the two circles, the pumping values are $\pm 2e/T$ while the outside is the nonquantized pump region. It is seen that for a stronger h_z , the region of $I_L = +2e/T$ is much larger than that of $I_L = -2e/T$. In Fig. 2(c), the valley degree below the crossing points $\pm K$ seems to vanish more easily since it almost converges with the band center point ($ka = 0$). This case is also clearly seen in Fig. 2(f) as well as its right inset. However, the valley degree is still conspicuous when the energy E is above the crossing points $\pm K$ from Figs. 2(c) and 2(f). Thus, the quantized value of $I_L = +2e/T$ seems to survive in the case of higher Fermi energy, shown in Fig. 6.

From the I_L - E relationship, the current is alternate from $I_L = +2e/T$ to $I_L = -2e/T$ and this is a typical property of the two-parameter pumping device, i.e., the pumped current satisfies the electron-hole antisymmetry since the pumping mechanism is related to the excitation of the electron-hole pairs from time-dependent perturbations. This is very different from the Thouless topological pump in which the pumping

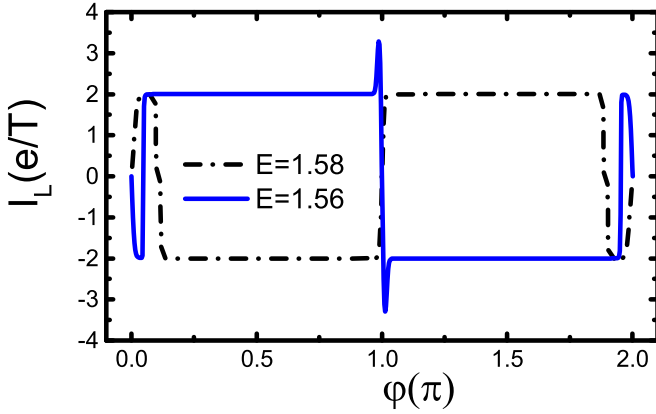


FIG. 7. Quantized pump current as a function of the pumping phase I_L - φ for two different Fermi energies. Other parameters are the same as those in Fig. 5(a).

results remain unchanged as long as the Fermi energy resides in the energy gap, because it equals the topological number of the whole insulator band below the Fermi energy that keeps unchanged within simply shifting E in the energy gap.

Another important characteristic of the two-parameter pump is the fact that the pumping depends crucially on phase φ . Based on the perturbation approximation, the formula [3] of an adiabatic pump is given by $I_L \sim \frac{\partial S}{\partial X_1} \frac{\partial S}{\partial X_2} \sin \varphi$ where S and $X_{1,2}$ are the scattering coefficients and the two pumping parameters, respectively. The current-phase relationship of the studied device is shown in Fig. 7 and it severely deviates from the normal sine function behavior. Instead, it displays a step-function formation: The pumped current can rapidly reverse its direction with variation of φ from the positive one ($2e/T$) to the negative one ($-2e/T$) or vice versa. The sine current-phase dependence of $I(\varphi)$ usually assumes that the system should be in a metallic phase and the transmission of electrons is nonzero in the cycle $t \in (0, T]$. This is clearly not the case we study here and, moreover, Eq. (5) is from the more rigorous Büttiker-Prère-Thomas (BPT) formula [39] of the adiabatic pump. As $\varphi = n\pi$ (n , integer), the pumping result deviates from the quantized one because, in this situation, the effective energy gap δ due to φ will be extremely small and E can easily locate outside the effective energy gap.

For the two-parameter pumping device studied above, it can be regarded as a two-domain device of $+h_z$ and $-h_z$ but not a uniform one. Therefore, the quantized pump cannot correspond to a topological invariant of a single phase. However, it is believed that the quantization of the system has its topological origin and should be protected by the topology of the each uniform h_z or $-h_z$ phase. As stated in Fig. 4(b), the topological interface states may arise in the energy gap and localize at the domain wall when \mathbf{h}_1 and \mathbf{h}_2 domains have the opposite sign or direction. They shall be robust against some moderate perturbations. Oppositely, as \mathbf{h}_1 and \mathbf{h}_2 point along the same direction (with the same sign) at some moments t , the interface state shall disappear. The time-evolution of this state can transport charges adiabatically from one end to the other end of the device; the physics is in nature similar to

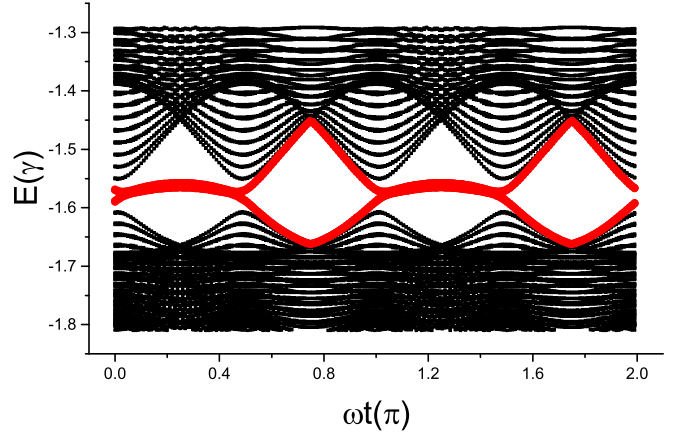


FIG. 8. Time evolution (ωt) of energy levels (E) in a self-closed NWS within a half $\mathbf{h}_1(t)$ and a half $\mathbf{h}_2(t)$. Only the levels around the bulk energy gap are plotted and the (red) solid line represents the interface states. Parameters are $h_z = t_{so} = 0.5\gamma$, $L = 120N_T$, $\varphi = \pi/2$, and $L_0 = 0$.

the end-state pumping charge in the Thouless topological pump.

In Fig. 8, we present the time evolution of the possible interface state in our device. It is seen that in some time intervals, this midgap state (red solid line) appears whereas it can evolve into the bulk state in other time region. The appearance or disappearance of the interface state with t in the bulk energy gap resembles a topological phase transition. Here, the calculation of the energy-band evolution is based on a self-closed device without leads, so the original end states due to a single h_z term in Fig. 4(b) are avoided in the display, which is not contributing to the pumping current. It is noted that the self-closed system is equal to the open device connected with the left and right leads [40]. The two times of crossing the bulk energy gap for the interface state (red solid line) in Fig. 8 represent the process that charges are moved from one end to the midinterface and then to the other end of the device. This is very different from the end-state evolution of the topological Thouless state where it crosses the gap only one time in a pumping cycle.

As mentioned above, the pumping quantization could occur when E resides in the effective energy gap δ , so the transmission through the device is prohibited $\mathcal{T} = 0$. As a result, the pumped charge in a cycle T is directly equal to the winding number of the reflection coefficient \mathcal{R} [42],

$$w = \frac{1}{2\pi i} \oint d\{\ln[\text{Det}(\mathcal{R})]\}, \quad (6)$$

where \mathcal{R} is a 2×2 matrix and $\text{Det}(\mathcal{R})$ represents the determinant of \mathcal{R} . One can directly use the continuum Eq. (4) to establish the scattering events of electrons to estimate \mathcal{R} . Here, we directly employ Eq. (1) to calculate \mathcal{R} by the Ando formula [41],

$$\mathcal{R}_{\alpha\beta} = \sqrt{\frac{v_\alpha}{v_\beta}} [U(-)^{-1} \{G_{ss}^r [G^r(ss)]^{-1} - I\} U(+)]_{\alpha\beta}, \quad (7)$$

where $v_{\alpha(\beta)}$ is the velocity of the $\alpha(\beta)$ spin eigenfunction in the lead, $U(\pm)$ is the left-going or right-going eigenfunction

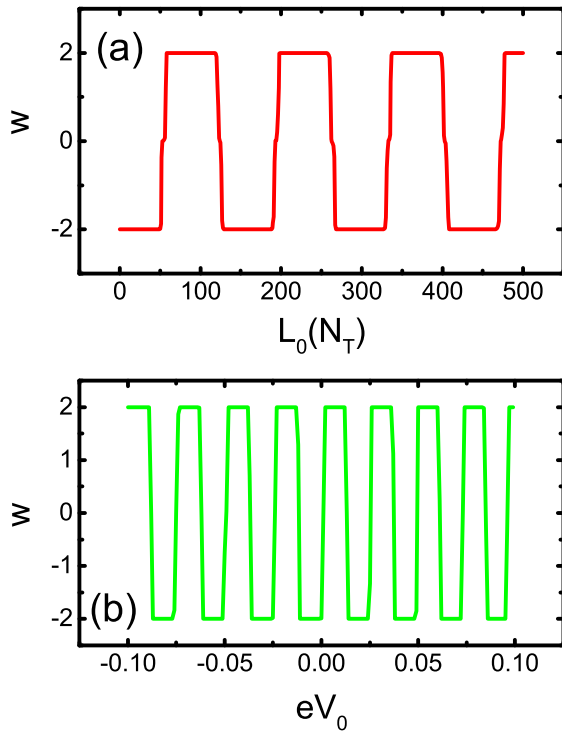


FIG. 9. Winding number of the reflection matrix as a function of the distance L_0 between two pumping sources and local potential eV_0 . Parameters are $h_z = t_{so} = 0.5\gamma$, $E = -1.59$, and $L_0 = 50N_T$ in (b).

matrix of the lead s ($= L, R$), I is the unit matrix, and G'_{ss} is the Green's function—same as the one in Eq. (5)—and is also dependent on the time t . $G'(ss)$ is the time-independent Green's function of a pure infinitely long lead s (not the half infinitely long for calculating the lead self-energy), in which no interaction like h_z in the scattering region is taken into account.

In Fig. 9(a), we present the winding number w as a function of the length L_0 between the two pumping potentials of the device. As is expected, w is shown to vary from $+2$ to -2 directly, which means the pumped charge is $\pm 2e$ in a periodicity T . 2 comes from two spin modes (degeneracy) involved in transport. Actually, when the phase of the reflection coefficient \mathcal{R} in electrodes advances by 2π in a pumping cycle but keeps its unit amplitude, the winding number of \mathcal{R} represents the charge number exiting from the device to the electrode and the pumping is therefore topologically protected.

The oscillation of w in Fig. 9(a) is also a significant property of the two-parameter pumping device, because the quantum interference will crucially affect the pumping results. However, the oscillation due to the quantum interference here is just a simple alternation from one constant to another constant. If there is a gate voltage V_0 applied onto the normal L_0 region, which modulates the dynamic phase of electrons transporting in the middle region where no h_z is applied, the pumping results shall display the similar step-function behavior. In Fig. 9(b), the winding number is plotted as a function of eV_0 and the alternation between ± 2 is indeed very clear. Hence, the quantum interference effect can provide

abundant adjustments of the quantized two-parameter charge pump unlike the Thouless topological pump.

IV. DISCUSSION AND CONCLUSION

We have discussed the possible charge-pump quantization in a two-parameter pump device, which is vitally dependent on materials with a strong spin-orbit interaction. A semiconductor nanowire like InAs [43] with the Rashba spin-orbit interaction is a suitable material candidate, since it has been extensively and intensively investigated, especially for recent research of Majorana fermions in experiments [44] where the Zeeman field was also demonstrated to open the energy gap of the nanowire. Although the InAs NWS has not been fabricated in experiments yet, there are plenty of experimental works [45–48] dedicated to the fabrication of other semiconductor NWS structures like SiC, SnO₂, and ZnO. For example, Xue *et al.* [48] developed a standard procedure to engineer in-plane silicon nanowire springs. This NWS with a spring structure is very applicable to our NWS model. Therefore, the fabrication of the InAs NWS is feasible in experiments with state-of-the-art techniques. Moreover, the InAs nanowire was also found to have significant flexibility [49], which is also suitable for fabricating a fold or bent NWS.

As for the time-dependent Zeeman fields utilized in our theory, one can use an AC electric field signal to control the corresponding magnetization through which electrons in our model feel the time-dependent Zeeman splittings, since a purely electric method to control the magnetism is currently mature in the multiferroic materials [50,51]. Besides, one can also directly use the microsolenoid to generate the AC magnetic field by controlling the AC electric current flowing through it. This may require that the NWS should thread through the microsolenoid and, meanwhile, the Zeeman field is along the wire direction (the y axis in Fig. 1). However, our model is also valid in this case, because the h_y field is the same as the h_z field in opening the bulk gap of the NWS and the average eigenspin direction of electrons in the NWS is along the x axis in the studied device. For the current folding NWS, the energy gap is estimated to about $\delta = 0.6$ MeV for the $N_T = 4$ case with these parameters like the effective mass of InAs $m^* = 0.023m_e$, the Rashba spin-orbit interaction strength 3×10^{-11} eV m, Lande g -factor $g \sim 15$, and the Zeeman field about 1 T.

Our study further confirms that if the pumping potentials can cause a topological phase, no matter what topological phase (with or without a boundary/end state) and no matter what the electron type (Dirac non-Dirac), the two-parameter pump device can generate an integer number of electron charges transported outside the device as long as the Fermi energy is devised in the effective energy gap δ . Moreover, this pump can be accounted for by the emergent interface state, which is protected by the bulk energy gap opened by the pumping potentials. Therefore, the pumping quantization should survive in moderate disorder or temperature effect, and this is helpful for experimental observations.

In summary, we have investigated the possible quantized pump in a traditional two-parameter pump device, which is based on a 1D NWS with the Rashba spin-orbit interaction. It is shown that the electronic structure of the system within

a superlattice structure from periodic folding exhibits new band-crossing structures, which can be gapped by a perpendicular Zeeman field. The two time-dependent Zeeman fields with a phase lag between them will give rise to a quantized pump: An integer number of electron charge can be pumped out adiabatically when the Fermi energy of the system lies in the energy gap opened by the Zeeman field. The time evolution of the emergent interface state in the energy gap is responsible for an integral charges pumped from one end of the device to the other end. The current direction is also sensibly dependent on system parameters such as the

Fermi energy, the pumping phase, and the dynamic phase of electrons transporting between two pumping sources.

ACKNOWLEDGMENTS

This work is supported by the Robert A. Welch Foundation under Grant No. E-1146 and the Texas Center for Superconductivity at the University of Houston. J.W. would also like to acknowledge support from the China Scholarship Council and NSFC (No. 11574045), J.F.L. thanks support from NSFC (No. 11774144).

-
- [1] B. L. Altshuler and L. I. Glazman, *Science* **283**, 1864 (1999).
- [2] M. Switkes, C. M. Marcus, K. Campman, and A. C. Gossard, *Science* **283**, 1905 (1999).
- [3] P. W. Brouwer, *Phys. Rev. B* **58**, 10135(R) (1998).
- [4] J. P. Pekola, O. P. Saira, V. F. Maisi, A. Kemppinen, M. Möttönen, Y. A. Pashkin, and D. V. Averin, *Rev. Mod. Phys.* **85**, 1421 (2013).
- [5] M. W. Keller, A. L. Eichenberger, J. M. Martinis, and N. M. Zimmerman, *Science* **285**, 1706 (1999).
- [6] I. M. Mills, P. J. Mohr, T. J. Quinn, B. N. Taylor, and E. R. Williams, *Metrologia* **43**, 227 (2006).
- [7] B. Wang, J. Wang, and H. Guo, *Phys. Rev. B* **67**, 092408 (2003).
- [8] B. Wang, J. Wang, and H. Guo, *Phys. Rev. B* **65**, 073306 (2002).
- [9] Y. Wei, J. Wang, and H. Guo, *Phys. Rev. B* **62**, 9947 (2000).
- [10] M. W. Keller, J. M. Martinis, and R. L. Kautz, *Phys. Rev. Lett.* **80**, 4530 (1998).
- [11] I. L. Aleiner and A. V. Andreev, *Phys. Rev. Lett.* **81**, 1286 (1998).
- [12] B. Kaestner, C. Leicht, V. Kashcheyevs, K. Pierz, U. Siegner, and H. W. Schumacher, *Appl. Phys. Lett.* **94**, 012106 (2009).
- [13] M. R. Connolly, K. L. Chiu, S. P. Giblin, M. Kataoka, J. D. Fletcher, C. Chua, J. P. Griffiths, G. A. C. Jones, V. I. Fal'ko, C. G. Smith, and T. J. B. M. Janssen, *Nat. Nanotech.* **8**, 417 (2013).
- [14] B. Kaestner and V. Kashcheyevs, *Rep. Prog. Phys.* **78**, 103901 (2015).
- [15] D. J. Thouless, *Phys. Rev. B* **27**, 6083 (1983).
- [16] A. Saha, D. Rainis, R. P. Tiwari, and D. Loss, *Phys. Rev. B* **90**, 035422 (2014).
- [17] D. Rainis, A. Saha, J. Klinovaja, L. Trifunovic, and D. Loss, *Phys. Rev. Lett.* **112**, 196803 (2014).
- [18] Y. E. Kraus, Y. Lahini, Z. Ringel, M. Verbin, and O. Zilberberg, *Phys. Rev. Lett.* **109**, 106402 (2012); M. Verbin, O. Zilberberg, Y. E. Kraus, Y. Lahini, and Y. Silberberg, *ibid.* **110**, 076403 (2013).
- [19] L. Wang, A. A. Soluyanov, and M. Troyer, *Phys. Rev. Lett.* **110**, 166802 (2013); X. Cai, L. J. Lang, S. Chen, and Y. Wang, *ibid.* **110**, 176403 (2013).
- [20] P. Marra, R. Citro, and C. Ortix, *Phys. Rev. B* **91**, 125411 (2015).
- [21] M. Lohse, C. Schweizer, O. Zilberberg, M. Aidelsburger, and I. Bloch, *Nat. Phys.* **12**, 350 (2016).
- [22] S. Nakajima, T. Tomita, S. Taie, T. Ichinose, H. Ozawa, L. Wang, M. Troyer, and Y. Takahashi, *Nat. Phys.* **12**, 296 (2016).
- [23] R. Citro, *Nat. Phys.* **12**, 288 (2016).
- [24] W. Ma, L. Zhou, Q. Zhang, M. Li, C. Cheng, J. Geng, X. Rong, F. Shi, J. Gong, and J. Du, *Phys. Rev. Lett.* **120**, 120501 (2018).
- [25] J. E. Avron, A. Elgart, G. M. Graf, and L. Sadun, *Phys. Rev. B* **62**, 10618(R) (2000).
- [26] Y. Makhlin and A. D. Mirlin, *Phys. Rev. Lett.* **87**, 276803 (2001).
- [27] Y. Levinson, O. Entin-Wohlman, and P. Wölfle, *Physica A* **302**, 335 (2001).
- [28] O. Entin-Wohlman and A. Aharony, *Phys. Rev. B* **66**, 035329 (2002).
- [29] J. Wang and J. F. Liu, *Phys. Rev. B* **95**, 205433 (2017).
- [30] Y. A. Bychkov and E. I. Rashba, *J. Phys. C* **17**, 6039 (1984).
- [31] E. B. Sonin, *Adv. Phys.* **59**, 181 (2010).
- [32] P. Gentile, M. Cuoco, and C. Ortix, *Phys. Rev. Lett.* **115**, 256801 (2015).
- [33] C. Ortix, *Phys. Rev. B* **91**, 245412 (2015).
- [34] S. Pandey, N. Scopigno, P. Gentile, M. Cuoco, and C. Ortix, *Phys. Rev. B* **97**, 241103(R) (2018).
- [35] A. H. Castro Neto, F. Guinea, N. M. R. Peres, K. S. Novoselov, and A. K. Geim, *Rev. Mod. Phys.* **81**, 109 (2009).
- [36] D. Xiao, W. Yao, and Q. Niu, *Phys. Rev. Lett.* **99**, 236809 (2007).
- [37] M. Ezawa, *Phys. Rev. B* **88**, 161406(R) (2013); *New J. Phys.* **14**, 033003 (2012).
- [38] M. P. Anantram, M. s. Lundstrom, and M. E. Nikonov, *Proc. IEEE* **96**, 1511 (2008).
- [39] M. Büttiker, A. Prêtre, and H. Thomas, *Z. Phys. B: Condens. Matter* **94**, 133 (1994).
- [40] G. M. Graf and G. Ortelli, *Phys. Rev. B* **77**, 033304 (2008).
- [41] T. Ando, *Phys. Rev. B* **44**, 8017 (1991).
- [42] J. E. Avron, A. Elgart, G. M. Graf, and L. Sadun, *J. Stat. Phys.* **116**, 425 (2004).
- [43] D. Liang and X. P. Gao, *Nano Lett.* **12**, 3263 (2012).
- [44] A. Das, Y. Ronen, Y. Most, Y. Oreg, M. Heiblum, and H. Shtrikman, *Nat. Phys.* **8**, 887 (2012).
- [45] J. Duan, S. Yang, H. Liu, J. Gong, H. Huang, X. Zhao, R. Zhang, and Y. Du, *J. Am. Chem. Soc.* **127**, 6180 (2005).
- [46] Z. Yang, Y. J. Wu, F. Zhu, and Y. Zhang, *Physica E* **25**, 395 (2005).
- [47] P. X. Gao, Y. Ding, W. Mai, W. L. Hughes, C. Lao, and Z. L. Wang, *Science* **309**, 1700 (2005).
- [48] Z. Xue, M. Xu, X. Li, J. Wang, X. Jiang, X. Wei, L. Yu, Q. Chen, J. Wang, J. Xu, Y. Shi, K. Chen, and P. R. i. Cabarrocas,

- [Adv. Funct. Mater.](#) **26**, 5352 (2016); Z. Xue, T. Dong, Z. Zhu, Y. Zhao, Y. Sun, and L. Yu, [J. Semicond.](#) **39**, 011001 (2018).
- [49] X. Li, X. L. Wei, T. T. Xu, Z. Y. Ning, J. P. Shu, X. Y. Wang, D. Pan, J. H. Zhao, T. Yang, and Q. Chen, [Appl. Phys. Lett.](#) **104**, 103110 (2014).
- [50] J. Krempaský, S. Muff, J. Minár, N. Pilet, M. Fanciulli, A. P. Weber, E. B. Guedes, M. Caputo, E. Muller, V. V. Volobuev, M. Gmitra, C. A. F. Vaz, V. Scagnoli, G. Springholz, and J. H. Dil, [Phys. Rev. X](#) **8**, 021067 (2018).
- [51] F. Matsukura, Y. Tokura, and H. Ohno, [Nat. Nanotech.](#) **10**, 209 (2015).